+ MODEL

HOSTED BY

ELSEVIER

Available online at www.sciencedirect.com

ScienceDirect

Karbala International Journal of Modern Science xx (2016) 1–5

http://www.journals.elsevier.com/karbala-international-journal-of-modern-science/

Impedance and modulus spectroscopy of ZrO_2–TiO_2–V_2O_5 nanocomposite

N. Padmamalini [a,*], K. Ambujam [b]

[a] *Department of Physics, St. Joseph Institute of Technology, Chennai 119, Tamilnadu, India*

[b] *Dr. Ambedkar Govt. Arts College, Chennai 39, Tamilnadu, India*

Received 21 August 2016; revised 28 September 2016; accepted 4 October 2016

Abstract

High-k ZrO_2–V_2O_5–TiO_2 nanocomposite prepared by coprecipitation-calcination method was investigated by impedance and modulus spectroscopy over a frequency range of 50 Hz–5 MHz, for different temperatures. Distinct peaks at characteristic frequencies were obtained. The shifting of the peaks towards high frequency with increase in temperature indicated a temperature dependent relaxation in the nanocomposite. Complex impedance formalism showed that the maximum value of the impedance decreases as temperature increases suggesting that the sample had negative temperature coefficient of resistance. The electric analysis confirms the findings of the impedance analysis. The f_{max} values for Z'' and M'' are different confirming non-Debye type of relaxation. The values of activation energies based on impedance and modulus relaxation were calculated and were equal to 1.02 eV and 0.51 eV respectively.

Keywords: Nanocomposite; Impedance analysis; Nyquist plots; Electric modulus

1. Introduction

Polycrystalline dielectric layers in any electronic device are subjected to alternating fields. The grain boundary interface and the metal electrode interface play an important part in their electrical response. Impedance spectroscopy is an attractive method used to distinguish between the bulk and boundary effects. This technique enables us to study the individual electrical properties of component parts of a material, thereby enabling us to modify the material in a favourable manner. It deals with the measurement of the real and imaginary parts of the impedance Z at various temperatures and frequencies. The impedance plots are in the form of semicircles that are associated with the grain boundary (R_{gb}) and bulk resistances (R_b). The effect of the intergrain and intragrain impedance plays a dominant role in deciding the material for a high-k dielectric layer. Zirconia and its composites have been studied extensively with respect to its applications in catalysis, SOFCs, dental and structural ceramics, dielectric layers on electronic devices etc [1–8]. The use of zirconia based materials as high-k dielectrics for gate dielectrics has been explored widely. Dielectric properties of binary oxides of Zirconium and titanium individually and with other

* Corresponding author.
E-mail address: sirishaaa73@gmail.com (N. Padmamalini).
Peer review under responsibility of University of Kerbala.

http://dx.doi.org/10.1016/j.kijoms.2016.10.001

dopants have been explored previously [9,10]. The addition of V_2O_5 to dielectric materials enhanced their dielectric properties [11,12]. A number of methods have been used to synthesize nanomaterials, but the simplest and effective method for synthesizing nanopowders is a wet chemical method. This method has been widely used in recent times to effectively synthesize nanomaterials [13,14]. In our previous study the morphology, optical and basic dielectric behaviour of the ZrO_2–TiO_2–V_2O_5 nanocomposite, synthesized by a coprecipitation method, were discussed [15]. A high dielectric permittivity of around 3000 was obtained. Here, the impedance spectroscopy and electric modulus analysis of the nanocomposite are studied and the results are discussed in detail.

2. Experimental details

A simple coprecipitation-calcination method was used to prepare the nanocrystalline ZrO_2–V_2O_5–TiO_2 composite [16–18]. Zirconium oxychloride, titanium tetrachloride and vanadium oxide (AR grade) were taken in the molar ratio 1:1:1 and dissolved in double distilled water. The water solution of $ZrOCl_2$, $TiCl_4$ and V_2O_5 was treated with aqueous ammonia at a pH of 9. This results in the formation of NH_4Cl. The hydrogel obtained was washed with distilled water to remove NH_4Cl and dried at 110 °C for 5 h in a hot air oven to a constant mass. Further, the samples were calcined at 700 °C in a furnace for 10 h. The synthesized samples were collected and powdered for characterization. A HIOKI 3532 LCR HITESTER instrument was used for obtaining the impedance parameters.

3. Results and discussion

3.1. Impedance analysis

The impedance of the material can be calculated using the formula [19].

$$Z(j\omega) = Z' - jZ'' = \frac{1}{1/R + j\omega C} = \frac{R}{1 + j\omega RC} = \frac{R}{1 + (\omega RC)^2} - \frac{j\omega R^2 C}{1 + (\omega RC)^2} \quad (1)$$

where $\omega = 2\pi f$, is the angular frequency, R is the resistance and C is the capacitance.

The variation of real part of the impedance with frequency and temperature of the ZrO_2–V_2O_5–TiO_2 nanocomposite is shown in Fig. 1(a) and (b). The high value of Z' at low frequencies is due to space charge polarization. It is evident that the impedance curves merge at higher frequencies (Fig. 1(a)), denoting that the real part of impedance (Z') is independent of temperature at higher frequencies. This behaviour indicates the dominance of space charge polarization, which occurs at low frequencies and also suggests a reduction in the barrier. The decrease in impedance at higher frequencies may be attributed to the hopping of electrons between localized ions [12]. At peak temperature the impedance values increase with decreasing frequency (Fig. 1(b)). This may be due to the accumulation of charges at grain boundaries.

Fig. 2(a) and (b) show the imaginary part of the impedance (Z'') with respect to frequency. It can be seen that Z'' reaches a maximum at a particular frequency, f_{max}. The maximum frequency (f_{max}) increases with increase in temperature. The maximum value of the impedance decreases as temperature increases. Hence it is evident that the material has a negative temperature coefficient of resistance (NTCR). Here again the impedance curves merge at higher frequencies, irrespective of the temperature. Broadening of the impedance peaks with increasing temperature may be due to a temperature dependent relaxation mechanism.

The effect of temperature on the impedance can be clearly understood from the Nyquist plots shown in Fig. 3(a) and (b). The intercepts of the semicircles on low frequency end gives the bulk resistance (R_b) of the sample at different temperatures [13]. The frequency at the maximum of the semicircle is equal to

$$\omega = 1/RC \quad (2)$$

The relaxation time is given by

$$\tau = RC \quad (3)$$

Therefore

$$\omega\tau = 1 \quad (4)$$

The values of the bulk or grain resistance (R_b) and the corresponding bulk capacitance (C_b) for the sample at different temperatures are given in Table 1. The presence of a single semicircle denotes a deviation from an ideal Debye behaviour [13]. The impedance plots shown can be represented by a parallel R–C combination shown in Fig. 3(a), where R and C represent the bulk resistance and capacitance respectively.

Please cite this article in press as: N. Padmamalini, K. Ambujam, Impedance and modulus spectroscopy of ZrO_2–TiO_2–V_2O_5 nanocomposite, Karbala International Journal of Modern Science (2016), http://dx.doi.org/10.1016/j.kijoms.2016.10.001

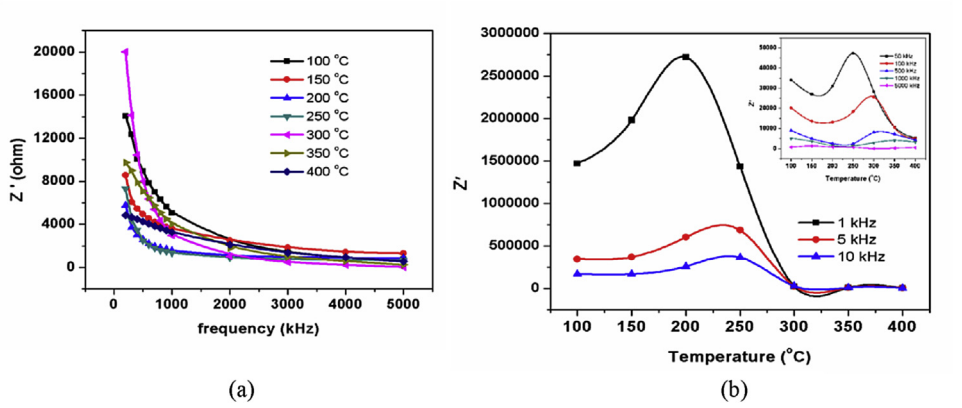

Fig. 1. (a) & (b): Variation of real part of impedance with frequency and temperature for $ZrO_2-V_2O_5-TiO_2$ nanocomposite.

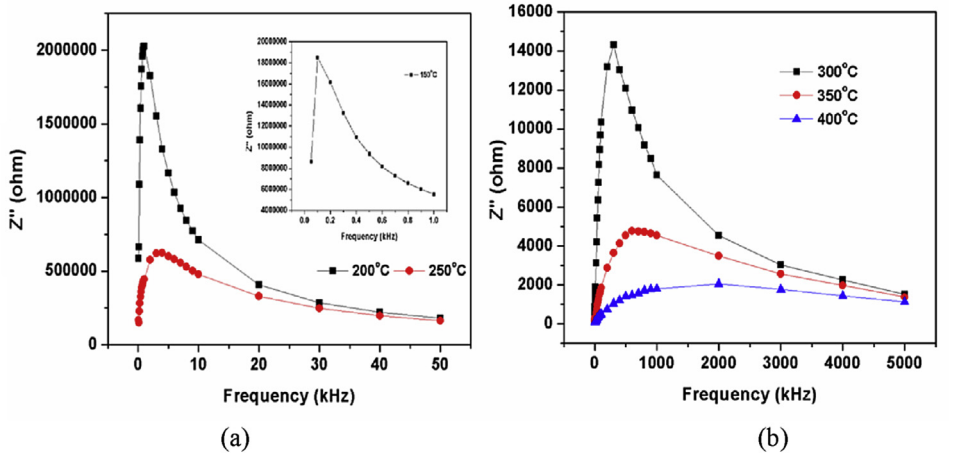

Fig. 2. (a) & (b): Variation of imaginary part of impedance with frequency for $ZrO_2-V_2O_5-TiO_2$ nanocomposite.

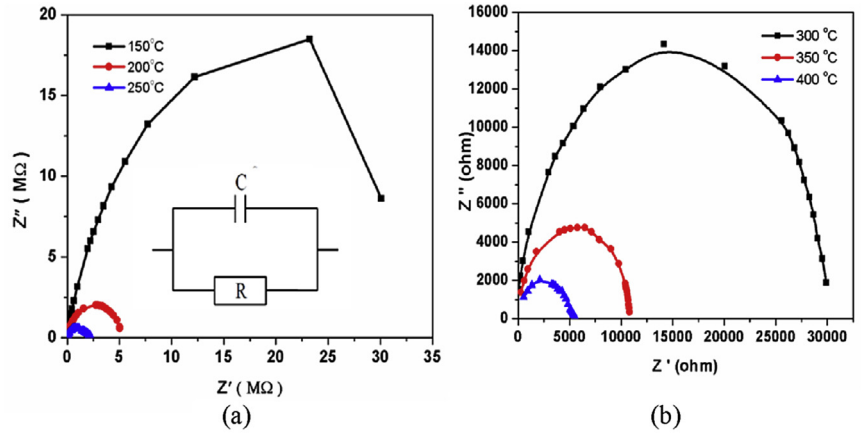

Fig. 3. (a) & (b): Nyquist plots of $ZrO_2-V_2O_5-TiO_2$ nanocomposite.

Please cite this article in press as: N. Padmamalini, K. Ambujam, Impedance and modulus spectroscopy of $ZrO_2-TiO_2-V_2O_5$ nanocomposite, Karbala International Journal of Modern Science (2016), http://dx.doi.org/10.1016/j.kijoms.2016.10.001

Table 1
Calculated values of bulk resistance and capacitance.

Temperature (°C)	R_b (ohm)	C_b (Farad)
150	3.4×10^7	4.6834×10^{-11}
200	5.2×10^6	3.0622×10^{-11}
250	2.2×10^6	1.8095×10^{-11}
300	3.1×10^4	1.6759×10^{-11}
350	1.07×10^4	2.4775×10^{-11}
400	6.1×10^3	1.2954×10^{-11}

3.2. Modulus analysis

Impedance plots highlight the resistive elements in the material, whereas the modulus plots highlight the capacitive elements, because the maximum of M″ is equal to $\varepsilon_o/2C$. The imaginary part of the electric modulus is calculated using the formula [14].

$$M'' = \frac{\varepsilon''}{(\varepsilon')^2 + (\varepsilon'')^2} \quad (5)$$

The variation in M″ with frequency at different temperatures is shown in Fig. 4(a) and (b). The plots exhibit pronounced relaxation peaks for M″. The low frequency side of the peak represents the frequencies for which charge carriers are mobile over a long range and can successfully hop from one defect site to another. The high frequency side of the peak signifies the frequencies for which the charge carries are confined to their potential wells and no long range motions are possible [15]. Here the peaks shift towards higher frequencies as the temperature increases. As a consequence it can be inferred that the relaxation time given by $\tau = 1/2\pi f_{max}$ decreases as temperature increases. Therefore the relaxation process is temperature dependent. The plots also indicate a change in both M''_{max} as well as in f_{max}, which denotes a change in C values with temperature [16]. The increase in M″ with temperature indicates the decrease in the value of the capacitance. But above 300 °C the value of M″ remains nearly the same. This may be due to an increase in the permittivity. For ideal Debye behaviour, the f_{max} values for Z″ and M″ at any given temperature should be the same. But for this sample f_{max} values are different, hence confirming non-Debye type of relaxation.

It is falsely assumed that all dielectric relaxations have the same relaxation time, irrespective of the function chosen to display it. Each dielectric function, like ac conductivity, impedance and electric modulus has a different relaxation time and activation energy [16]. The activation energies calculated from an

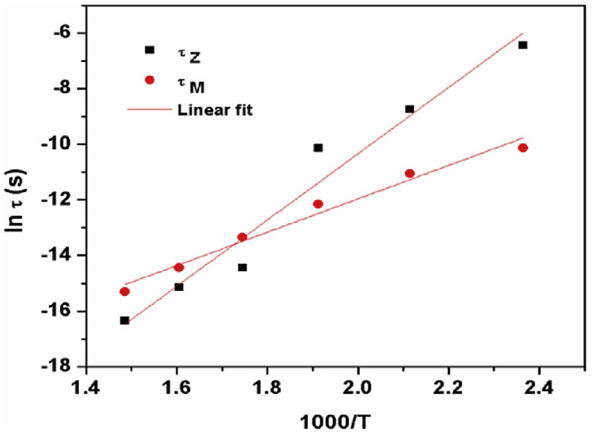

Fig. 5. Variation of relaxation times for impedance and modulus with temperature.

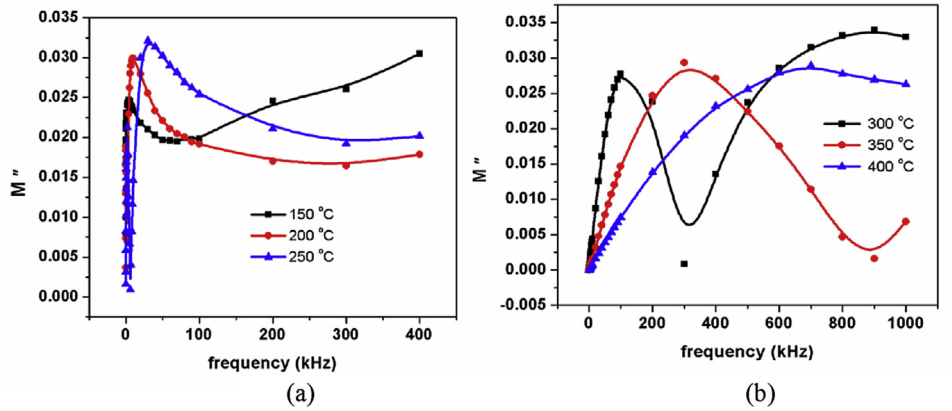

Fig. 4. (a) & (b): Variation of imaginary part of impedance with frequency for $ZrO_2-V_2O_5-TiO_2$ nanocomposite.

Please cite this article in press as: N. Padmamalini, K. Ambujam, Impedance and modulus spectroscopy of $ZrO_2-TiO_2-V_2O_5$ nanocomposite, Karbala International Journal of Modern Science (2016), http://dx.doi.org/10.1016/j.kijoms.2016.10.001

Arrhenius plots for Z″ and M″ (Fig. 5) for the sample was 1.02 eV and 0.51 eV respectively. It can be seen that the activation energy calculated from the impedance spectra is different from that of the modulus spectra. This suggests that the relaxation processes are not due to the same type of charge carriers. The activation energy calculated in a previous study [9] using ac conductivity was 0.3 eV. The difference in activation energies indicates that charge carriers have to overcome different energy barriers while conducting and relaxing. This variation in the activation energies also emphasizes that the relaxation processes are of the non-Debye type.

4. Conclusion

The impedance and modulus formalisms for the ZrO_2–V_2O_5–TiO_2 nanocomposite were studied over a range of temperatures and frequencies. The plots for variation of Z″ and M″ with frequency exhibited peaks which moved towards the high frequency region with increase in temperature, which may be due to a temperature dependent relaxation. The decrease in the magnitude of the impedance with temperature denotes a negative temperature coefficient of resistance. The Nyquist plots exhibit a single semicircle, which is due to the dominance of bulk phenomena. Both modulus and impedance formalisms depict a non-Debye type of relaxation. The high impedance of the nanocomposite along with its high dielectric permittivity make it suitable for application as a gate dielectric.

References

[1] J.R. Kelly, I. Denry, Stabilized zirconia as a structural ceramic: an overview, Dent. Mater 24 (2008) 289–298.
[2] R.H.J. Hannink, P.M. Kelly, B.C. Muddle, Transformation toughening in Zirconia- containing ceramics, J. Am. Ceram. Soc. 83 (3) (2000) 461–487.
[3] M.K. Patil, A.N. Prasad, B.M. Reddy, Zirconia- based solid acids: green and heterogeneous catalysts for organic synthesis, Curr. Org. Chem. 15 (2011) 3961–3985.
[4] H.-J. Eom, M.-S. Kim, D.-W. Lee, Y.-K. Hong, G. Joeng, K.-Y. Lee, Zirconia catalysts (ZrO_2 and Na-ZrO_2) for the conversion of phenethyl phenyl ether (PPE) in supercritical water, Appl. Catal. A Gen. 493 (2015) 149–157.
[5] E.-O. Oh, C.-M. Whang, Y.-R. Lee, J.-H. Lee, K.J. Yoon, B.-K. Kim, J.-W. Son, J.-H. Lee, H.-W. Lee, Thin film yttria-stabilized zirconia electrolyte for intermediate-temperature solid oxide fuel cells (IT-SOFCs) by chemical solution deposition, J. Eur. Ceram. Soc. 32 (8) (2012) 1733–1741.
[6] C. Ko, K. Kerman, S. Ramanathan, Ultra-thin film solid oxide fuel cells utilizing un-doped nanostructured zirconia electrolytes, J. Power Sources 213 (2012) 343–349.
[7] P. Kondaiah, G.M. Rao, S. Uthanna, Preparation of magnetron sputtered ZrO_2 films on Si for gate dielectric applications, J. Phys. Conf. Ser. 390 (2012) 012031.
[8] Y.M. Park, A. Desai, A. Salleo, L. Jimison, Solution-processable Zirconium Gate Dielectrics for flexible organic field effect transistors operated at low voltages, Chem. Mater. 25 (13) (2013) 2571–2579.
[9] M. Dong, H. Wang, C. Ye, L. Shen, Y. Wang, J. Zhang, Y. Ye, Structure and electrical properties of sputtered TiO_2/ZrO_2 bilayer composite dielectrics upon annealing in nitrogen, Nanoscale Res. Lett. 7 (2012) 31–36.
[10] S. Arunprathap, A. Napolean, C.R. Azariah, Fabrication of thin film transistor using high K dielectric materials, Int. J. Eng. Comput. Sci. 3 (2014) 5387–5391.
[11] G.-H. Chen, H.-R. Xu, M.-H. Jiang, Effect of vanadium doping on sintering and dielectric properties of strontium barium niobate ceramics, J. Mater. Sci. 21 (2010) 168–172.
[12] Z. Yan, J.L. Huang, Y.J. Gu, B. Jin, R.Y. Wang, Effects of V_2O_5 addition on the microstructure and microwave dielectric properties of $ZnNb_2O_6$ ceramics, Adv. Mater. Res. 476–478 (2012) 940–943.
[13] K. Kaviyarasu, E. Manikandan, J. Kennedy, M. Maaza, A comparative study on the morphological features of highly ordered MgO: AgO nanocube arrays prepared via a hydrothermal method, RSC Adv. 5 (2015) 82421–82428.
[14] K. Kaviyarasu, D. Premanand, J. Kennedy, E. Manikandan, Synthesis of Mg doped TiO_2 nanocrystals prepared by wet chemical method: optical and microscopic studies, Int. J. Nanosci. 12 (2013) 1350033–1350039.
[15] N. Padmamalini, K. Ambujam, Structural and dielectric properties of ZrO_2–TiO_2–V_2O_5 nanocomposites prepared by co-precipitation calcination method, Mater. Sci. Semicond. Process 41 (2016) 246–251.
[16] W. Pyda, N. Moskala, A zirconia composite with in-situ synthesized titanium diboride inclusions, in: Proceedings of the 16th International Conference on Composite Materials, Kyoto Jpn, 2007, pp. 1–7.
[17] M.M. Hessien, M.M. Rashad, K. El-Barawy, Controlling the composition and magnetic properties of strontium hexaferrite synthesized by co-precipitation method, J. Magn. Magn. Mater 320 (2008) 336–343.
[18] A. Ataie, S. Heshmati-Manesh, Synthesis of ultrafine particles of strontium hexaferrite by a modified co-precipitation method, J. Eur. Ceram. Soc. 21 (2001) 1951–1955.
[19] B.H. Venkataraman, K.B.R. Varma, Microstructural, dielectric, impedance and electric modulus studies on Vanadium doped and pure Strontium bismuth niobate ($SrBi_2Nb_2O_9$) ceramics, J. Mater. Sci. 16 (6) (2005) 335–344.

Please cite this article in press as: N. Padmamalini, K. Ambujam, Impedance and modulus spectroscopy of ZrO_2–TiO_2–V_2O_5 nanocomposite, Karbala International Journal of Modern Science (2016), http://dx.doi.org/10.1016/j.kijoms.2016.10.001